Renewable Energy 246 (2025) 122835

Contents lists available at ScienceDirect

Renewable Energy

journal homepage: www.elsevier.com/locate/renene

One-pot depolymerization of forest residues to potential aviation fuel over hybrid zeolite – N-doped activated carbon supported NiMo catalyst

Quoc Khanh Tran [a,c,*], Muhammad Abdus Salam [a], Phuoc Hoang Ho [a], Huy Xuan Le [a], Christian Kugge [b], Derek Creaser [a], Louise Olsson [a,**]

[a] Chemistry and Chemical Engineering Department, Competence Centre for Catalysis, Chalmers University of Technology, SE-412 96, Gothenburg, Sweden
[b] SCA R&D Centre, Sundsvall, Sweden
[c] Institute of Energy and Technology - Electrochemical Process Engineering (IET-4), Julich Research Center, Germany

ARTICLE INFO

Keywords:
Hybrid support
Waste forest residue
Sawdust
YNAC
Bimetallic catalyst

ABSTRACT

In this work, sawdust and bark are depolymerized by catalytic reductive liquefaction using a bimetallic NiMo catalyst, with the aim to generate bio-fuel components in a single reaction step, that potentially could be used to produce sustainable aviation fuel (SAF). The hybrid support Zeolite Y combined with N-doped on activated carbon (YNAC) was synthesized from zeolite Y (silica/alumina ratio, SAR = 80) and N-doped activated carbon (NAC). The effect of temperature, pressure, and catalyst loading were systematically investigated to obtain conditions favorable for the yield and quality of the liquid product. The result at 400 °C, 20 bar H_2 (at room temperature), 4 h residence time with 30 wt% catalyst loading of NiMo@YNAC (75:25) showed the lowest solid yields, which was 3.9 wt% when using sawdust. The solid yield increased to 18.2 wt% when using bark and was intermediate (8.4 wt%) when using a sawdust/bark blend with 8/2 wt ratio. Sawdust was mainly converted into a liquid product consisting of cycloalkanes (C_4-C_7) (48.1 wt%), aromatics (2.1 wt%), phenolic compounds (15.8 wt%), and a heavy oil fraction (9.2 wt%). Meanwhile, bark was converted into similar compounds, however, with higher yields of mainly naphthenic and biphenyl components. The catalytic activity of NiMo on other supports such as ϒ-Al_2O_3, ZrO_2, TiO_2, and CeO_2 were also examined at the same conditions as NiMo@YNAC (75:25). Moreover, acidic washing of the bark was very beneficial resulting in that the solid yield significantly decreased, from 18 % to 6 %, while the bio-oil yield was improved (from 78 % to 91 %). The results showed that the NiMo@YNAC (75:25) catalyst with high deoxygenation and hydrogenation effects is a promising candidate for depolymerization of biomass into biofuels.

1. Introduction

Biomass is considered the most abundant and renewable material in the world [1–3]. For decades, biomass has been receiving a lot of attention regarding the production of fuels and chemicals [4,5]. Among biomass types, waste forest residue (e.g., sawdust, bark), which is generated during wood harvesting and processing has a large potential for generating liquid fuels. Especially in the scope of green chemistry and biorefining, biomass can be fractionated into different types of products such as gas, liquid fuel, and solids (biochar) [6,7]. Depending on the targeted products, different technologies (pyrolysis [1], gasification, liquefaction [8], fractionation [9]) have been studied widely.

Reductive catalytic liquefaction (RCL) is a promising method to produce high quality bio-oils [10,11]. It offers several advantages such as the usage of wet biomass as raw feedstock that reduces the energy needed and additional steps for removing the moisture content before use. Also, since it employs hydrogen, catalytic hydrodeoxygenation can improve the quality of the liquid bio-oil by lowering the oxygen content in the bio-oil. Brandner et al. [10] investigated solvolysis with methanol at 225 °C produces native-like lignin from poplar, enabling the study of intrinsic lignin properties and evaluation of steady-state lignin depolymerization. Ebikade et al. [11] reported RCL to depolymerize, over Ru/C powder and Ru/Al_2O_3 pellets, five herbaceous biomass feedstocks into phenolic monomers with high yields (~40 wt% based on total (Klason +

* Corresponding author. Chemistry and Chemical Engineering Department, Competence Centre for Catalysis, Chalmers University of Technology, SE-412 96, Gothenburg, Sweden.
** Corresponding author.
E-mail addresses: Qu.tran@fz-juelich.de (Q.K. Tran), louise.olsson@chalmers.se (L. Olsson).

https://doi.org/10.1016/j.renene.2025.122835
Received 3 December 2024; Received in revised form 11 February 2025; Accepted 7 March 2025
Available online 14 March 2025

acid soluble) lignin and >50 wt% when stabilized using aldehydes), leaving behind a carbohydrate pulp residue. In addition, RCL can extract and disassemble lignin from the lignocellulose matrix via hydrogenolysis, forming phenolic monomers with high yield, through a combination of suitable solvent and specific catalysts under hydrogen conditions while still retaining most of the holocellulose fraction [12,13]. Anderson et al. [12] studied the RCL of corn stover using carbon-supported Ru and Ni catalysts at 200 and 250 °C in methanol and obtained 27.2 (250 °C) and 28.3 % (200 °C) of monomer yields, respectively, with Ni/C catalyst.

Catalysts based on noble metals such as Pd, and Ru have been commonly used for RCL processes due to their higher activity, selectivity, and stability in comparison to more lower cost options [14–16]. Vangeel et al. [14] reported the fractionation of black locust bark could be divided into three phases: (i) a solid phase that mostly consisted of carbohydrates and leftover lignin; (ii) an aqueous phase; and (iii) an oil phase that contained lignin mono-, di-, and oligomers as well as aliphatic, suberin-derived monomers. The highest bark oil yield was obtained at 35.1 wt% with Pd/C at 250 °C, 2 h and at 20 bar H_2 pressure. Muangmeesri et al. [15] investigated RCL of hemp using Pd/C and formic acid in MeOH/H_2O with the addition of ρ-toluenesulfonic acid to yield 38.8 wt % of monophenolic compounds. Li et al. [16] found that a Ru/C catalyst at 300 °C showed the highest conversion; with the liquid alkylcyclohexanes yield reaching 97.2 % (based on lignin monomers in cornstalk) with 52.7 % polyols (24.5 % sorbitol, 12.2 % xylitol, and 16.0 % C_2–C_4 polyols) at 200 °C. The synergistic effect between Ru and RuO_2 species in the conversion of lignocellulosic biomass led to hydrogenation (Ru) and efficient cleavage of the lignin–carbohydrate (RuO_2) interlinkages and promotion of the retro-aldol condensation of carbohydrates. However, the cost of noble metal catalysts for this process is one of the biggest issues hindering the further development of RCL technology to pilot scale using noble metals.

Several studies using alternative catalysts have been investigated which have lower price than noble metal catalysts, and a large focus has been on less active non-noble metals especially nickel catalysts [17,18]. Klein et al. [17] showed that dihydroeugenol (DHE) and 2,6-dimethoxy-4-propyl-phenol (DMPP) exhibited selectivity of 22 and 67 % to produce isoeugenol (i-EuOH) and methoxyisoeugenol (Mi-EuOH), respectively, using 5 wt% Ni/C. Furthermore, depending on the biomass substrate, the overall yields of lignin-derived compounds vary from less than 10 % to more than 30 %. Song et al. [18] studied lignin depolymerization (LDP) in methanol using various catalysts such as Ni/C, Ni/Al_2O_3, Cu/C, activated carbon (AC), and Ni/SBA-15. The best selectivity for monomeric phenols was achieved at 50 % conversion of birch wood lignin with Ni/C. It is noteworthy that the transformation of solid lignin over the solid Ni/C catalyst is characterized by the first fragmentation of lignin into smaller lignin species via alcoholysis reactions, with molecular weights ranging from approximately 1100 to 1600 m/z (ratio mass to charge). These smaller fragments are then transformed into monomeric phenols via the Ni/C catalyst. However, with the scalability of the RCL process, lower temperatures, and hydrogen pressures, the risk of non-noble metal catalysis becoming rate limiting is higher under certain conditions, which could require increasing the catalyst loading [13,19]. The ideal catalyst should be low in cost to enable large-scale production, have high activity and selectivity to ensure complete catalytic conversion of lignin intermediates into specific stabilized products, and maintain high catalytic performance over time.

Recently developed N-doped activated carbon (NAC) materials have been used for studying Ni/NAC for the conversion for guaiacol. NAC is considered a promising catalyst support due to the improvement in hydrophilicity and basicity of the support, which could improve the interaction between substrate and support in an aqueous system [20]. In addition, NAC has a large surface area which allows for high metal dispersion [21,22]. NAC also can have various pore sizes for different applications and optimization of carbon-based catalysts depends on different raw materials and/or activation methods [23]. Zeolite based catalysts have been typically used in thermal processes to convert biomass feedstocks to alcohols, ketones, acids, furans, phenolic and aromatic compounds [24,25]. Among those products, aromatic compounds are the main component in typical aviation fuel. The production of aviation fuel range aromatics from biomass has been shown to be increased over zeolite-based catalysts [24,26].

However, according to our knowledge, there are no studies available that have examined bark utilization in the RCL process using either nickel or molybdenum-based catalysts. Therefore, driven by cost reduction and to increase the effectiveness of the catalyst, in this study we have for the first time developed a hybrid N-doped activated carbon mixed with zeolite (YNAC) supported bimetallic NiMo catalyst (NiMo@YNAC), which were compared with other NiMo catalysts. NiMo@YNAC was synthesized by a combination of wet impregnation and hydrothermal synthesis. The effect of catalyst loading, catalyst composition, reaction conditions (temperature and pressure, and time), and effect of bark addition were studied.

2. Experimental

2.1. Catalyst synthesis

Activated carbon (AC) (powder), and melamine (M) were purchased from Sigma Aldrich. The zeolite that was used in this study was a commercial zeolite Y (H type, Zeolyst International) with silica to alumina ratio (SAR) = 80. The synthesis process of the hybrid support containing zeolite and N-doped activated carbon (named as YNAC) is shown in Fig. S1. Activated carbon (AC) was mixed with melamine (M) into a solution with various weight ratios of AC:M (2.5:1, 5:1, 7.5:1, and 10:1) for 1 h. Then the mixture was dried in an oven for 12 h at 105 °C to remove moisture. After that, the mixture was placed in a ceramic crucible and put into a tubular quartz reactor. The mixture was purged with Ar flow during 30 min before heating to remove the air inside of the reactor. N-doped activated carbon (NAC) was synthesized at 800 °C using 400 NmL/min Ar flow for 2 h.

Next, the NAC material was mixed with zeolite (with different ratios) and about 30 mL of water in a Teflon liner for 1 h. Then the Teflon liner was put in an autoclave for synthesis of the hybrid support YNAC at 200 °C for 12 h at its autogenous pressure. The mixture after taking it out of the autoclave evaporated using a rotary evaporator at 65 °C. Then the mixture was dried in an oven for 12 h at 80 °C to remove the remaining moisture. Finally, the bimetallic NiMo@YNAC was prepared by a wetness impregnation method. The approriate amount of ammonium molybdate tetrahydrate (99 %, Sigma-Aldrich) and nickel (II) nitrate hexahydrate (99 %, Sigma-Aldrich) was dissolved in water and then applied dropwise to the hybrid support YNAC (with the aim to obtain 16 wt% of NiMo (1Ni:3Mo weight ratio). The mixture was then stirred for 1.5 h at 25 °C. Water was removed via rotary evaporation at 65 °C. The same amount of NiMo catalyst on other supports such as ϒ-Al_2O_3, ZrO_2, TiO_2, and CeO_2 were also synthesized by following the same wetness impregnation procedure. The resultant mixture was then oven-dried for 12 h at 80 °C and pretreated in Ar (with NAC support contained) at 500 °C (5 °C/min) or N_2 (with other supports) for 4 h. Before each utilization, the catalysts were reduced in an autoclave at 450 °C using 20 bar H_2 (at room temperature).

It should be noted that in this study, catalyst powders were used, in order to focus on the reactions and mechanisms, and minimize mass transfer. For upscaling, catalyst in the form of pellets and extrudates could have advantages for catalyst separation and recycling, but this was not the focus of the current study.

For regeneration steps, the spent catalyst was washed with acetone 3 times to remove contaminants and dried at 105 °C for 12 h. After that, the spent catalyst was placed in a ceramic boat in a horizontal-tubular quartz reactor. The spent catalyst was purged with Ar flow during 30 min before heating to remove the air inside of the reactor and heated up

at 600 °C using 400 NmL/min Ar flow or 1.4 ml/g-spent catalyst·h^{-1} for 2 h [31]. Note, the temperature should not be too high during regeneration to avoid oxidation of the activated carbon. The regenerated catalysts are named R1, R2, and R3 corresponding to the number of regeneration cycles.

2.2. Catalyst characterization

The specific surface area profiles of fresh, spent, and regenerated catalysts were measured using the Brunauer–Emmett–Teller (BET) and Barrett-Joyner-Halenda (BJH) methods. The hybrid support YNAC and NiMo@YNAC were dried under N_2 flow at 200 °C overnight before the measurements.

Inductively Coupled Plasma-Sector Field Mass Spectroscopy (ICP-SFMS, ALS Scandinavia AB, Luleå, Sweden) was performed to measure the metal loadings (Ni, Mo), and elemental analysis (EA) was utilized to determine the N-doped/AC ratio of the synthesized catalysts. The C, H, N, O analysis was mearsure using a Vario micro cube-Elementar instrument analyzer (Chalmers Materials Analysis Loboratory, Gothenburg, Sweden). Temperature programmed-desorption (TPD) of CO_2 and NH_3 were performed to measure the acidities and basicities of the impregnated catalysts following a method as described in previous studies [36]. X-ray diffraction (XRD) diffractograms were obtained via a Bruker AXSD8 Advance diffractometer operating at 40 kV and 40 mA with CuKα monochromatic radiation (λ = 1.542 Å) operating with a step size of 0.03° per second. Scanning electron microscopy (SEM) was conducted using a JEOL 7800F Prime to determine the morphology of catalysts. The fresh and spent catalysts were also analyzed by temperature programmed oxidation (TPO) using thermogravimetric analysis (TGA) in an oxygen atmosphere to study catalyst deactivation with ramping 10 °C/min from room temperature to 700 °C. For all catalyst characterization, samples that were calcined were used.

2.3. Experimental procedure for RCL experiments

The biomass that was used for valorization was both softwood sawdust and bark provided by SCA R&D Centre, Sundsvall, Sweden. In addition, a pretreatment of the bark sample was investigated by mixing bark with 5 % HNO_3 for 5 h and rinsing by water to remove the remaining HNO_3. After that, the pretreated bark was dried at 80 °C before use.

The RCL experiments were performed in an autoclave (300 mL, Parr Inc). The details regarding the autoclave were described in previous studies [27,28]. 3 g of biomass feedstock was mixed with catalyst (20 wt % based on the biomass feedstock) and 60 g of hexadecane, then added subsequently to the reactor. The reactor was purged with N_2 three times to remove the air inside the reactor and then with H_2 repeatedly. After that, the reactor was pressurized to the required H_2 pressure (from 20 to 35 bar) at room temperature and heated up to reaction temperature (from 350 to 400 °C) with a stirring rate of 1000 rpm using a magnetically driven internal stirrer. The experiment was run for 4h (the reaction time was measured from the moment when the target temperature was reached), then the reaction was stopped by cooling down again to room temperature.

The gas products were collected using a gas bag. The liquid product mixture was filtered using a filter glass 4 μm (ROBU, Germany) to remove the solid residue from the mixture. The mixture was filtered and named as the hexadecane fraction. The reactor after reaction was washed 3 times with acetone to remove a mixture of solid residue and liquid. Then the solid product was dried in an oven at 105 °C for 12 h. The rest of the organic phase rich in acetone and hexadecane was named as the acetone fraction. The hexadecane fraction was condensed at room temperature after 1 d to separate heavy compounds which sticked on the bottle wall. This heavy fraction was separated and combined with the acetone fraction. The acetone fraction was rotary evaporated at 180 °C to collect the total heavy fraction. The following equations were used to calculate by mass balances, the main product yields.

$$Gas = \frac{m_{gases} - m_{H2\ remaining}}{m_{biomass}} \times 100\ (wt\%) \quad (1)$$

$$Solid = \frac{m_{solid\ residue} - m_{catalyst}}{m_{biomass}} \times 100\ (wt\%) \quad (2)$$

$$Total\ Liquid\ oil = 100 - Gas - Solid\ (wt\%) \quad (3)$$

The heavy and monomer fractions of the liquid oil product are calculated by the following.

$$Heavy\ fraction\ (HF) = \frac{m_{heavy\ fraction}}{m_{biomass}} \times 100\ (\mathrm{wt\%}) \quad (4)$$

$$Light\ oil\ (LO) = 100 - Gas - Solid - HF - Water\ \ (wt\%) \quad (5)$$

The gas products were analyzed by a gas chromatograph (GC) (SCION 456, Bruker) equipped with both thermal conductivity (TCD) and flame ionization detectors (FID). Quantification of the gas sample was based on external calibrations of CO, CO_2, and hydrocarbons C_1-C_5. The water content in the liquid products was determined by Karl Fisher volumetric titration using a Metrohm 870 KF Titrino plus apparatus. The water content was determined using Karl Fischer titrant (HYDRANAL™ - Composite 5, Honeywell Fluka™) and dry methanol (Honeywell Fluka™). This water content was measured based in the total liquid (included hexadecane) and then the water yield from biomass liquefaction was calculated by excluding the hexadecane mass. The heavy fraction was diluted and analyzed using 2D (^{1}H-^{13}C) HSQC (Heteronuclear single quantum coherence spectroscopy) NMR with a setup of a Bruker Avance III HD; Bruker BioSpin GmBH, Rheinstetten, Germany. Data processing was further conducted using Bruker Topspin software. The liquid product obtained was analyzed by a 2D GC × GC-MS-FID (7890B–5977A, Agilent) instrument using VF-1701MS (30 m × 250 μm × 0.25 μm) and DB-5MS (3 m × 150 μm × 0.15 μm) columns. GC Image software was used to analyze the evolved 2D chromatograms (MS/FID). The quantification of the detected products was made using external calibrations for different groups of products taking 1,4-dioxane as an internal standard. The GC detected yield of liquid components was determined using the following equation:

$$GC\ Detected\ Liquid\ Yield = \frac{amount\ of\ product\ (g)}{biomass\ feedstock\ (g)} \times 100\ (wt\%) \quad (6)$$

The molecular weight distribution was measured by gel permeation chromatography (GPC). The heavy fraction was mixed with dimethyl sulphoxide (DMSO) before analysis to get good dilution. The GPC system used DMSO with 10 mM LiBr as the eluent, and was calibrated with pullulan standards in the range 0.180–708 kDa. Two detectors were measured in series: an ultraviolet (UV) detector operating at 280 nm and a refractive index (RI) detector.

3. Results and discussion

3.1. Biomass characterization

The waste forest residues including softwood sawdust, bark and their mixtures were provided by SCA (Sweden) and grinded to <0.2 mm before use (Fig. S2). Analysis included ash, moisture, volatile matter, and fixed carbon of the sawdust (Table 1) and the results were 0.2 ± 0.05, 11.3 ± 0.06, 75.0, and 13.5 wt% (followed ASTM E1755, E1756, and E872-82), respectively. The ash, moisture, volatile matter, and fixed carbon of the bark were 3.0 ± 0.14, 9.00 ± 0.06, 63.2, and 24.8 wt%, respectively. Through elemental analysis (EA), the C, H, N, O, and S of the sawdust sample were 49.1, 6.5, 0.03, 44.4, and 0.002 wt%, respectively. The C, H, N, O, and S of the bark sample were 54.6, 6.0, 0.3, 37.5, and 1.6 wt%, respectively. The inorganic elements found in the bark material were mainly K (2220.0 ppm), Ca (7510.0 ppm), along with

Table 1
Proximate, ultimate and ICP analysis of biomass sample.

Biomass		Sawdust	Bark
Proximate analysis (wt% on dry basis)	Moisture [a]	$11.3_{\pm 0.06}$	$9.0_{\pm 0.06}$
	Ash [b]	$0.2_{\pm 0.05}$	$3.0_{\pm 0.14}$
	Volatile matter [c]	75.0	63.2
	Fixed carbon [d]	13.5	24.8
Ultimate analysis (wt% on dry basis)	C	49.1	54.6
	H	6.5	6.0
	N	0.03	0.3
	S	0.002	1.6
	O[e]	44.4	37.5
HHV (MJ/kg)[a]		20.2	22.3
ICP analysis (mg/Kg)	K	374.0	2220.0
	Na	<200.0	<200.0
	Ca	820.0	7510.0
	Mg	114.0	828.0
	Al	<100.0	739.0

[a] ASTM E1756, Standard test method for determination of total solids of biomass.
[b] ASTM E1755, Standard test method for determination of ash content of biomass.
[c] ASTM E872-82, Standard test method by thermogravimetric analysis.
[d], [e] By difference.
[a] HHV = (33.5 × [C]+142.3 × [H]-15.4 × [O]-14.5 × [N]) × 10-2 MJ/kg (Demirbas [29]).

trace amounts of other metals such as Mg, Al, Ca, Fe. Meanwhile, the inorganic content in the sawdust sample was lower, with K (374.0 ppm), Ca (820.0 ppm), and traces of other metals (Mg, Al, Ca, Fe).

Thermogravimetric analysis (TGA) was utilized to figure the decomposition pattern of the wood sawdust material, and the results are displayed in Fig. S3. The decomposition temperature range for the wood sawdust material was from 200 to around 580 °C. Meanwhile, this temperature range for bark material was wider from 150 to around 650 °C. The maximum decomposition (T_{max}) of the wood sawdust and bark occurred at around 368 and 350 °C, respectively.

3.2. Characterization of the catalysts

The BET profiles of the NiMo catalysts on different supports are shown in Table 2 and Fig. S4. Among all the catalysts, the NiMo catalyst supported on activated carbon (NiMo@NAC) exhibited the highest BET surface area (644.4 m^2/g) and pore volume (0.69 cm^3/g), while the catalyst supported on Ceria (NiMo@CeO_2) had the lowest BET surface area (6.5 m^2/g) and pore volume (0.03 cm^3/g). The NiMo@γ-Al_2O_3 catalyst had a BET surface area of 150.5 m^2/g, which was lower than that of the NiMo@Y (593.8 m^2/g) and NiMo@NAC catalysts, but higher than that of all the other catalysts on pure metal oxide supports. The

Table 2
Pore structure data of the NiMo catalyst on various supports.

Sample	BET Surface Area (m^2/g)	Pore Size (nm)	Pore volume (cm^3/g)
NiMo@Y	593.8	2.4	0.27
NiMo@NAC	644.4	3.6	0.69
NiMo@YNAC(75:25)	210.2	4.8	0.30
NiMo@YNAC(25:75)	493.6	3.7	0.46
NiMo@YNAC(50:50)	384.6	4.2	0.49
NiMo@γ-Al_2O_3	150.5	7.8	0.37
NiMo@ZrO_2	7.0	14.5	0.03
NiMo@TiO_2	9.0	11.0	0.03
NiMo@CeO_2	6.5	12.8	0.03
Spent-NiMo@YNAC (75:25)	77.0	6.8	0.16
R1	214.0	6.9	0.23
R2	176.4	6.8	0.12
R3	66.1	6.9	0.03

NiMo catalysts supported on YNAC (NiMo@YNAC(75:25), NiMo@YNAC(25:75), and NiMo@YNAC(50:50)) showed intermediate BET surface areas and pore volumes. The NiMo@γ-Al_2O_3 catalyst had the largest pore size (7.8 nm), while the NiMo@NAC catalyst had the smallest pore size (3.6 nm) among all the Y and/or NAC supported catalysts. The NiMo@NAC catalyst, which exhibited the highest BET surface area and pore volume, may be a promising catalyst for the depolymerization of biomass due to its high surface area and pore volume. However, the small pore size of NiMo@NAC may limit the diffusion of reactants and products, which could potentially reduce the catalytic activity. The NiMo@γ-Al_2O_3 catalyst, which had the largest pore size, may provide better diffusion properties, but its lower BET surface area and pore volume may reduce its overall activity. The NiMo@ZrO_2, NiMo@TiO_2, and NiMo@CeO_2 catalysts examined in this work all exhibited relatively low BET surface areas, pore sizes, and pore volumes, which may limit their potential as catalysts for the depolymerization.

XRD patterns of NiMo on various supports are shown in Fig. 1. With the YNAC, Y, NAC, γ-Al_2O_3, and CeO_2 supports there were no peaks of Ni and Mo found. This might be due to the high dispersion of the NiMo catalyst on those supports [28]. On the TiO_2 and ZrO_2, MoO_3 was found at 23.2, 25.6, 27.2, 38.5, 12.7, and 49.0°. $NiMoO_4$ was observed by the peaks at 28.7, 25.2, 43.9, 14.3, and 32.5°. Especially, $Zr(MoO_4)_2$ was found at 23.0, 30.6, and 50.1° on NiMo@ZrO_2.

The results of the scanning electron microscopy with energy-dispersive X-ray (SEM-EDX) analysis for the Y and NAC supported catalysts are presented in Fig. 2(a-d). EDX dot mapping clearly illustrated that Ni, and Mo were dispersed uniformly on the surface of both supports, and the results for NiMo@YNAC are shown as an example. The NiMo@Y showed conglomeration of the particles, while both NiMo@YNAC and NiMo@NAC showed amorphous shapes of particles.

The TPR, CO_2-TPD, and NH_3-TPD profiles are shown in Fig. 3(A). The TPR profile of the NiMo catalyst on YNAC (75:25) showed the lowest reduction temperature at about 460 °C. The NiMo@Y and NiMo@γ-Al_2O_3 had higher temperature reduction peaks at about 500 °C while NiMo on other supports such as TiO_2, ZrO_2, and CeO_2 required much higher temperatures of about 600 °C to be reduced. This can affect the hydrogenolysis/deoxygenation activities of catalysts since the reaction temperature varied from 350 to 400 °C and the maximum reduction temperature in our reactor system was fixed at 450 °C. This indicates that the NiMo catalyst should be in it least reduced state using the TiO_2, ZrO_2, and CeO_2 supports.

The CO_2 desorption temperature and the degree of basicity are correlated, and the basic sites can be categorized according to their strength, in relation with the CO_2 desorption temperature peaks as: (i) weak (50–200 °C), (ii) intermediate (200–400 °C), and (iii) strong (400–650 °C) [30]. The basic active sites can catalyze a variety of processes, including carbon coupling (C-C) reactions, which change low molecular weight molecules like organic acids, aldehydes, and ketones into chemicals used in the production of diesel and gasoline [31,32]. Moreover, while acidic catalyst sites favor synthesis of CO, the formation of CO_2 from deoxygenation of pyrolysis vapors is promoted by basic catalysts. The NiMo@YNAC(75:25) showed a CO_2 desorption peak starting from 370 °C and extending to more than 600 °C, and simultaneously with a significantly higher concentration, which shows a high basicity compared to NiMo on the other supports (Fig. 3(B)). The temperature at which NH_3 desorption occurred represents the potency of the catalyst's acid sites (Fig. 3(C)). The desorption peak at a low temperature (<250 °C) indicates weak acidity, while desorption peaks at higher temperatures indicate medium (250–400 °C) and strong acidity (400–650 °C). The amount and strength of acidic sites in the resulting catalyst affects their activity for depolymerization and oxygen removal and contributes to reactions such as hydrogenolysis, isomerization/transalkylation, hydrocracking, and dehydration [2,18]. The amount of acidity and strengths are shown in Table S1. Among the tested catalysts, NiMo@Y, NiMo@γ-Al_2O_3, and NiMo@YNAC (75:25) showed

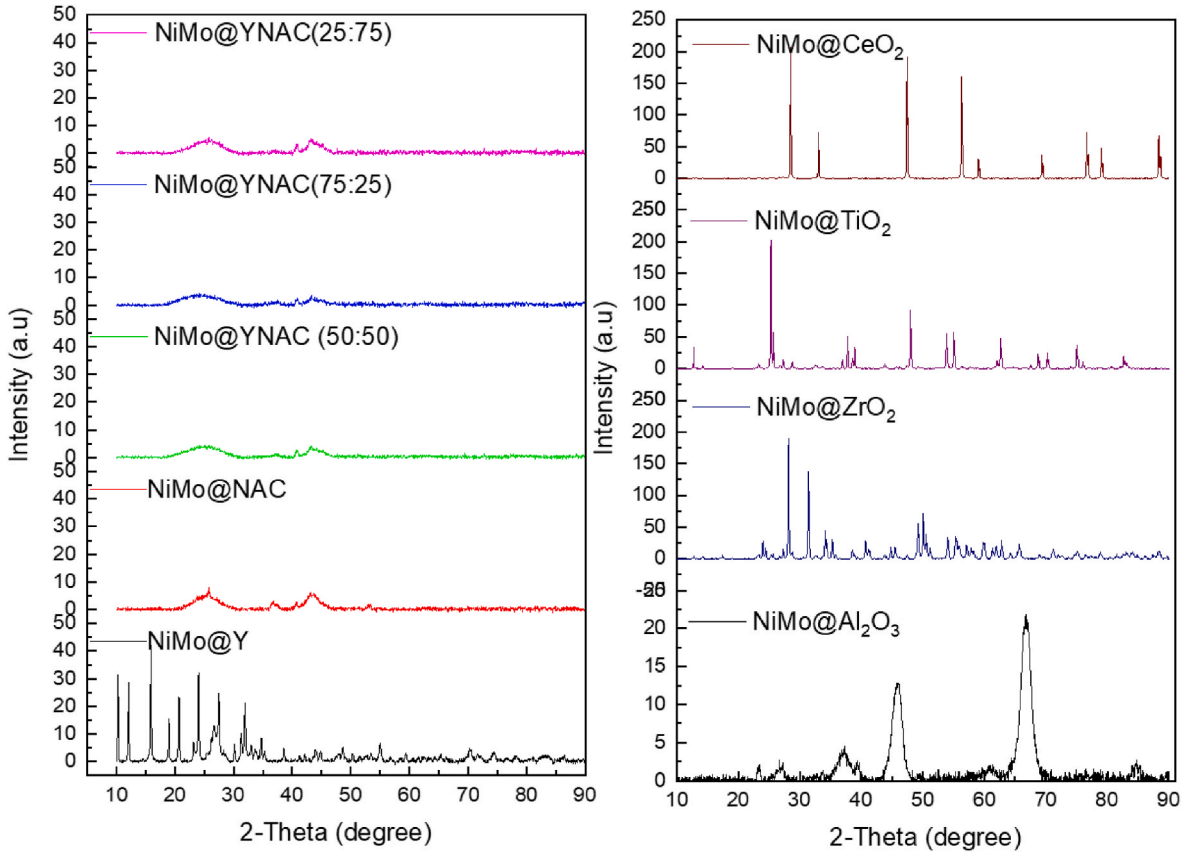

Fig. 1. XRD patterns of NiMo on various supports.

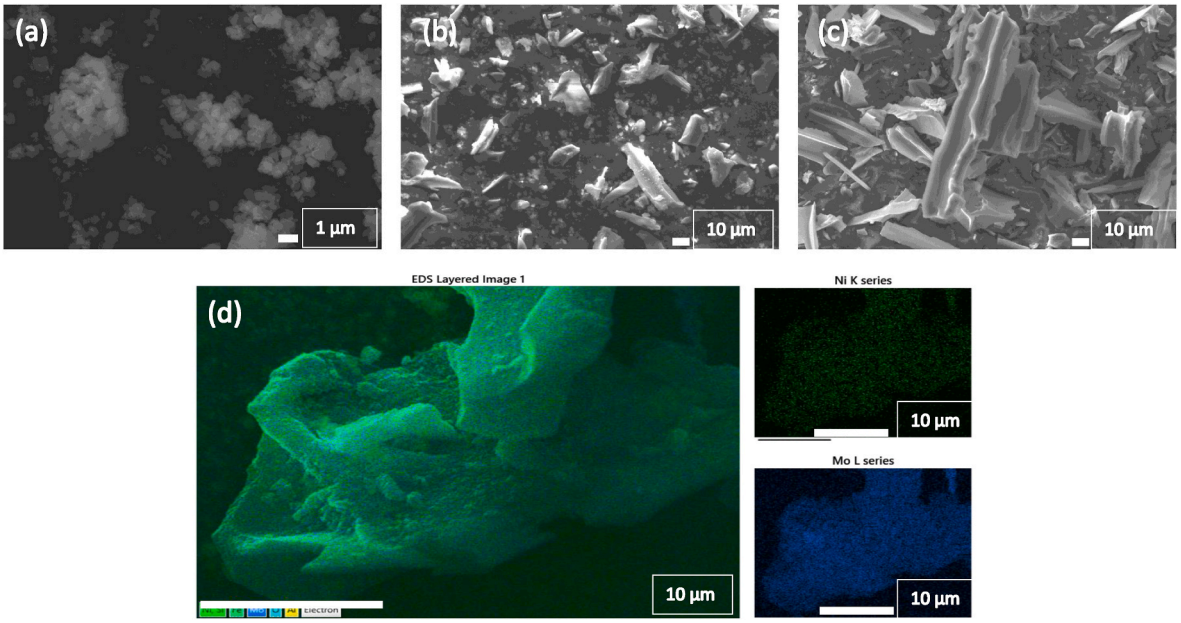

Fig. 2. SEM image of (a) NiMo@Y, (b) NiMo@YNAC (75:25), (c) NiMo@NAC, and (d) EDX dot-mapping of NiMo@YNAC (75:25).

much higher acidity than NiMo on other supports. NiMo@ϒ-Al_2O_3 showed the highest acid site density of 292.5 µmol/g in the weak and medium strength ranges. Meanwhile, NiMo@YNAC (75:25) had lower acidity with 221.3 µmol/g. However, it also had a small peak at around 550 °C indicating the presence of some sites with strong acidity. It should be noted that the YNAC support was prepared by using USY with a high SAR ratio of 80, which could explain why NiMo@YNAC had a slightly lower acidity compared to NiMo@ϒ-Al_2O_3. A unique feature of NiMo@YNAC (75:25) is that it combines both acid and basic sites, which could contribute to a high yield of mono-aromatic/cyclic compound in liquid products.

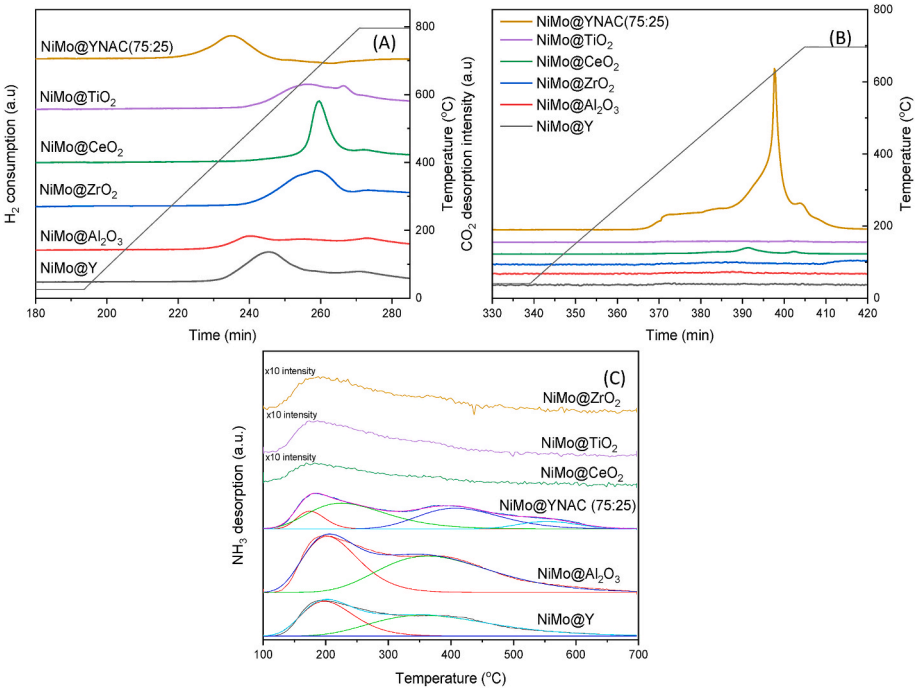

Fig. 3. Temperature programmed: (A) Reduction (TPR), (B) CO_2 desorption (CO_2-TPD), and (C) NH_3 desorption (NH_3-TPD) from NiMo on various supports.

3.3. *Effect of reaction conditions and NiMo catalyst on different supports*

Figs. 4 and 5 and Table S2 provide experimental results for depolymerization of the biomass using different catalysts and process conditions. The experimental conditions varied, including temperature and H_2 pressure. In general, high temperatures led to faster depolymerization reactions, as the increased energy helps to overcome activation energy barriers and promote the breaking of bonds in the biomass [33, 34]. However, the applied reaction temperature should not be too high in order to cause carbonization reactions and increasing the gas formation [35]. The reaction temperature was varied (350, 375 and 400 °C), which influenced the product distribution after 4h reaction for the sawdust liquefaction and hydrotreatment in hexadecane using a hydrogen pressure of 20 bar (at room temperature) with the

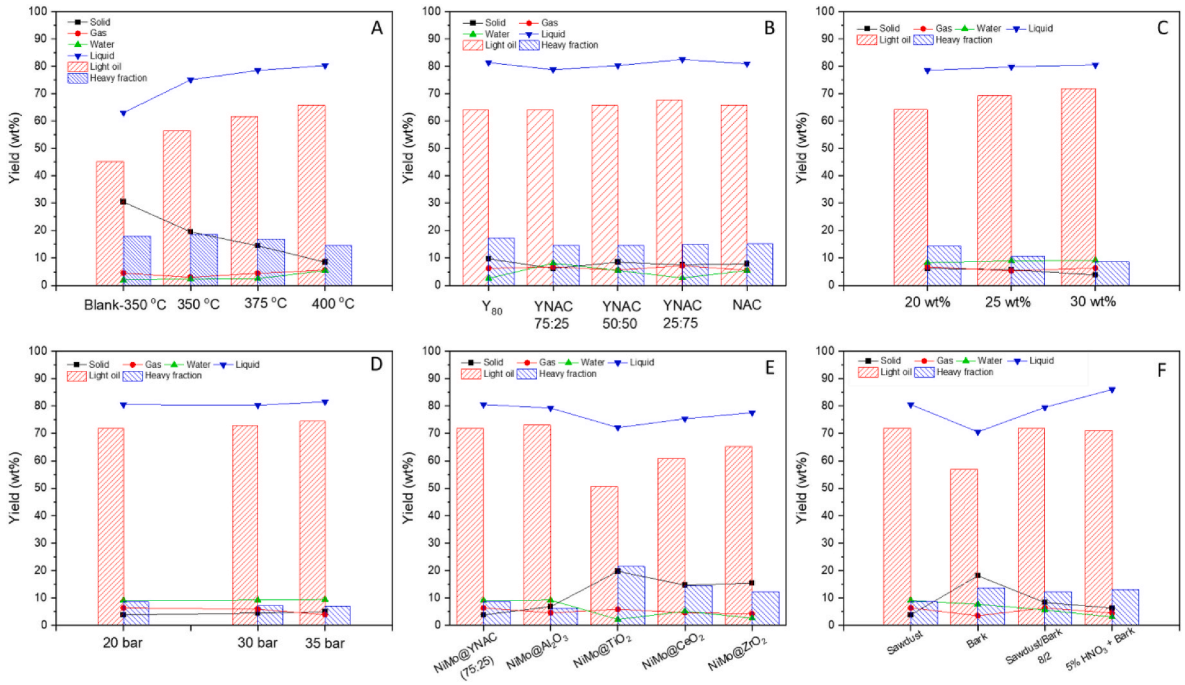

Fig. 4. Product distribution from sawdust and bark reductive catalytic depolymerization under various conditions: (A) Effect of reaction temperature at 20 wt% NiMo@YNAC (50:50), 20 bar H_2 (@room temperature), 4 h, 350–400 °C; (B) Effect of various ratio Y/NAC support at 20 bar H_2 (@room temperature), 4 h, 400 °C; (C) Effect of catalyst loading at NiMo@YNAC (75:25), 20 bar H_2 (@room temperature), 4 h, 400 °C; (D) Effect of different initial H_2 pressure at 30 wt% NiMo@YNAC (75:25), 4 h, 400 °C; (E) Effect of different supports at 30 wt% NiMo@YNAC (75:25), 20 bar H_2 (@room temperature), 4 h, 400 °C; (F) Effect of various biomass type at 30 wt% NiMo@YNAC (75:25), 20 bar H_2 (@room temperature), 4 h, 400 °C.

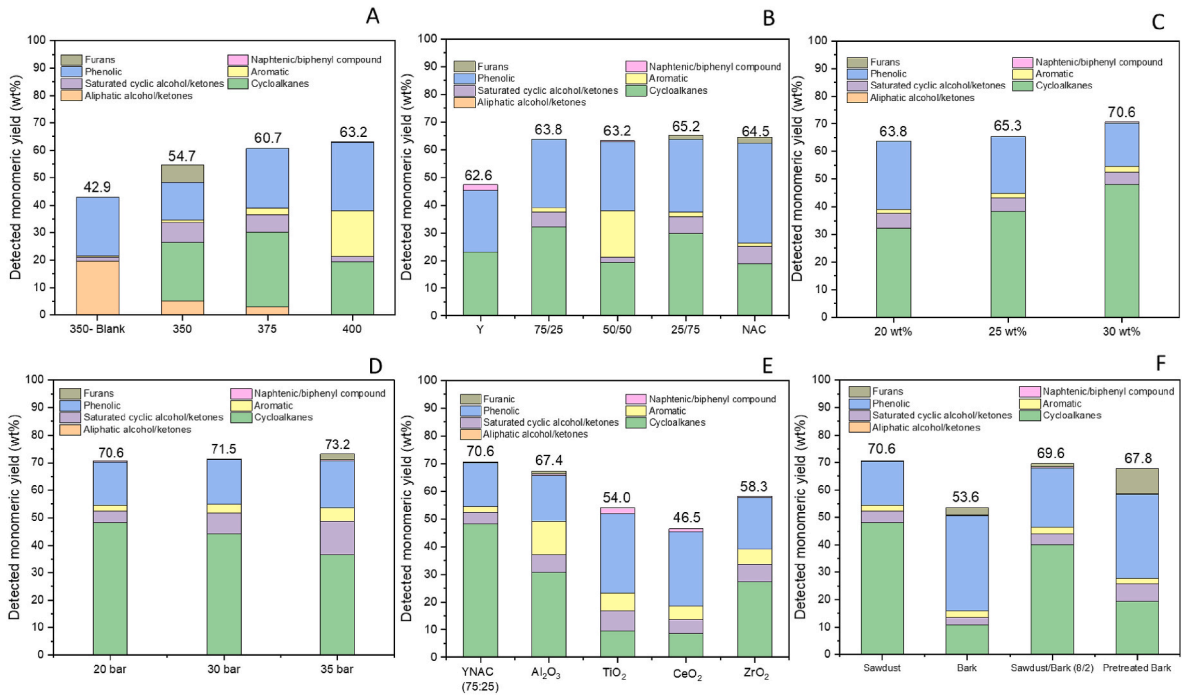

Fig. 5. GC Detected monomeric yield in liquid bio-oil under different conditions: (A) Effect of reaction temperature at 20 wt% NiMo@YNAC (50:50), 20 bar H_2 (@room temperature), 4 h, 350–400 °C; (B) Effect of various mass ratios Y/NAC support at 20 bar H_2 (@room temperature), 4 h, 400 °C; (C) Effect of catalyt loading at NiMo@YNAC (75:25), 20 bar H_2 (@room temperature), 4 h, 400 °C; (D) Effect of different initial H_2 pressure at 30 wt% NiMo@YNAC (75:25), 4 h, 400 °C; (E) Effect of different supports at 30 wt% NiMo@YNAC (75:25), 20 bar H_2 (@room temperature), 4 h, 400 °C; (F) Effect of various biomass type at 30 wt% NiMo@YNAC (75:25), 20 bar H_2 (@room temperature), 4 h, 400 °C.

NiMo@YNAC (50:50) catalyst (Fig. 4(A)). The liquid oil and gas yields increased, while the char formation decreased when increasing the temperature. Increasing the reaction temperature from 350 to 400 °C, resulted in the solid yield decreasing significantly from 19.5 to 8.5 wt%, respectively. In contrast, the liquid oil and gas yields increased from 77.4 to 85.9 wt% and from 3.0 to 5.7 wt%, respectively. The sawdust was decomposed and depolymerized into smaller molecules or fragments, and then the unstable fragments could react with reactive hydrogen atoms, mostly provided by H_2 dissociation on the surface of the catalyst, to form bio-oil. Thus, the yield of bio-oil and gas increased significantly with increasing temperature. Insyanni et al. [36] found the same phenomena in a study of the hydrodeoxygenation of lignin-derived oxygenates and biomass pyrolysis oil into hydrocarbon fuels using titania-supported nickel phosphide catalysts from 200 to 300 °C. The alkyl-methoxyphenol conversion and cycloalkane yields increased from 90 to 100 % and 45–87 %, respectively over the temperature range. Jaya et al. [3] studied the conversion of lignocellulosic biomass to ketones and aromatics over a multifunctional Cu–Ru/ZSM-5 catalyst. As the temperature increased from 260 to 300 °C, both the oakwood conversion and lignin-derived phenolic monomers (LDPM) and ketone (KN) yields increased. However, an increase in temperature to 320 °C resulted in a decrease in the LDPM and KN yields, which could be due to repolymerization of reaction intermediates or product cracking. The same conclusion was made by Chou et al. [8] from investigating the effect of temperature from 280 to 320 °C, where the highest bio-oil yield of about 45.2 % was obtained at the reaction temperature of 300 °C. Couto et al. [33] reported that the bio-oil yield increased with temperature until 325 °C, and then decreased at 350 °C in the study of hydrothermal liquefaction of biomass produced from domestic sewage treatment in high-rate ponds. Too high temperature could result in lower bio-oil yield, due to higher gas formation [37–39].

The influence of varying composition of the support was examined by varying the Y:NAC weight ratio, including 100:0; 75:25; 50:50; 25:75, and 0:100, respectively (Fig. 4(B)). Both the zeolite and activated carbon have unique properties that can contribute to the efficiency and selectivity of the process. Zeolite Y is a porous material with high surface area, providing acid sites that can help to promote the depolymerization of lignocellulosic materials [27,40]. Activated carbon, on the other hand, has high surface area and pore volumes, and in addition larger pore diameters compared to Zeolite Y, which can help to promote mass transfer [41,42]. Additionally, activated carbon provides basic sites that can help to reduce the formation of byproducts [21,43]. NiMo@Y resulted in the highest solid yield of 9.7 wt% at 400 °C. Meanwhile, NiMo@YNAC (75:25) showed the lowest solid yield of 6.3 wt%, respectively. When zeolites and activated carbon are used together as supports for NiMo, they can complement each other's properties and provide a synergistic effect on the depolymerization process. For example, the acid sites provided by the zeolite can help to promote the depolymerization reaction through proton donation and thus, stabilize the small fragments [28], while the basic sites provided by the activated carbon can help to reduce the formation of undesirable products.

The effect of catalyst loading was examined with 20, 25, and 30 wt% catalyst (based on dried biomass weight) with NiMo@YNAC (75:25), as shown in Fig. 4(C). In the absence of catalyst the char increased significantly, and the liquid oil yield decreased. Increasing the catalyst loading resulted in a decrease in the production of char and improved the liquid oil yield [34]. The char yield decreased from 6.3 to 3.9 wt%, whereas the liquid oil yield increased from 87.0 to 89.7 wt%, respectively. The gas yield was similar when increasing the catalyst loading, however, the gas selectivity changed, as shown in Fig. S5(C). The methane selectivity increased from 24.3 to 28.5 wt% (note hydrogen in the gas is not included in the selectivity) and other gas phase hydrocarbons from 13.9 to 19.8 wt%, whereas the CO selectivity decreased from 21.1 to 11.5 wt%, respectively. Meanwhile, the CO_2 selectivity stabilized at about 40 wt%, respectively.

The effect of hydrogen pressure on the depolymerization of biomass was examined by increasing the starting pressure at room temperature from 20 to 35 bar (Fig. 4(D)). This resulted in the total pressure

(including effect of solvent vaporization) in the reactor system at 400 °C reaching 45–75 bar, respectively. The solid yield slightly increased from 3.9 to 5.0 wt%, which showed that the effect of H_2 pressure was unintuitive [44]. Moreover, the gas yield decreased from 6.4 to 4.0 wt% and the liquid oil yield slightly increased from 89.7 to 91.0 wt%. The increase of the hydrogen pressure could suppress the formation of gas [40], which was observed. Moreover, the heavy fraction decreased when increasing the hydrogen pressure, suggesting that some of the heavy fraction was further reacted to form solids. However, it should be noted that the increase in solid formation is rather small, only about 1 wt%, thus the effect is small. Generally, increasing the hydrogen pressure can lead to an increase in the rate of depolymerization, since by increasing the hydrogen pressure, the concentration of hydrogen in the reaction mixture will be increased [34]. However, free radicals in the reaction system also can be saturated by other intermediates released by hydrocracking, assisted by high hydrogen pressure, and thus become prone to repolymerization of light fragments, leading to undesirable char formation [40,44]. In addition, secondary reactions of small fragments may be prevented by high pressure, resulting in a decrease in gas yield.

Due to the development of metal-support interactions (MSI), supports are a significant functional component that affect catalytic activity and selectivity in many heterogeneous catalytic reactions [45,46]. The most important elements in the effective tuning of MSI are the support composition, shape, doping, and surface changes. Other kinds of supports such as γ-Al_2O_3, TiO_2, CeO_2, ZrO_2 were used for the NiMo catalyst to compare to the hybrid support YNAC (75:25) at 400 °C, 20 bar, and 4h reaction time (Fig. 4(E)). TiO_2, CeO_2 and ZrO_2 all showed negative results compared to the hybrid support YNAC(75:25) due to their high solid product yields from 14.7 (CeO_2) to 19.8 wt% (TiO_2), respectively. These negative results might occur due to the low density of acid sites of the TiO_2, CeO_2 and ZrO_2 supported NiMo catalysts, as well as their low surface areas (Table 2). However, the usage of the conventional γ-Al_2O_3 as a support for NiMo in the depolymerization process was quite effective, where the solid, liquid, and gas product yields were 6.9, 88.5 and 4.6 wt%, respectively. However, the NiMo@YNAC (75:25) exhibited a better performance with only 3.9 % solids formed at the same conditions.

The catalyst NiMo@YNAC (75:25) was used to investigate its performance with different feedstocks including sawdust, bark, and a mixture of sawdust/bark (80/20 wt ratio) at the same conditions of 400 °C, 20 bar H_2 (room temperature) and 4 h reaction time (Fig. 4(F)). Compared to sawdust depolymerization, bark gave a significantly higher solid product yield of 18.2 wt%, whereas the gas yield was quite low at 3.6 wt%. Meanwhile, the blended sawdust/bark (80/20 wt %) feedstock showed less char yield (8.4 wt%) and a higher gas yield (5.2 wt%) compared to the bark results. The blended feedstock results were primarily related to the proportion of the weight fraction of sawdust and bark and seemed not to involve any interactions between the feedstocks. The higher solid yield and lower liquid oil yield with bark might be due to its higher inorganic content leading to deactivation or condensation reactions on the NiMo@YNAC in the depolymerization process. Inorganic minerals can act as catalytic poisons, which can reduce the activity and selectivity of the catalyst and lead to the formation of byproducts [47,48]. The ash, which is as much as 3 % in the bark (Table 1) will also likely remain in solid form and increase the solid formation. Additionally, the bark contained significantly less volatile matter, 63 % versus 75 % (see Table 1), which makes the depolymerize more difficult.

Moreover, the extractive fraction, which is higher in bark, can have an impact on the char formation [49,50]. The extractives can undergo thermal decomposition at high temperature and produce volatile products. These volatile products can then react with other components in the biomass or other intermediate products to form solid residues or char. Acid washing pretreatment of biomass prior to fast pyrolysis has been considered effective for removal of both ash and extractives [47,48]. An experiment using bark pretreated with 5 % HNO_3 for 5 h was also conducted to examine these assumptions. In this study, the result was improved significantly compared to the original bark result with the solid yield reduced to 6.3 wt%, and liquid oil yield increased to 89.1 wt %. Meanwhile, the gas yield increased slightly to 4.5 wt%. Specifically, Park et al. [48], whereby pretreating *Empty Fruit Bunch* (EFB) with dilute nitric acid, the total liquid yield was enhanced from 52.2 wt% to 63.9 wt % and the char yield was reduced from 41.9 wt% to 39.9 wt% compared to original EFB through the fast pyrolysis process. The same trend was observed in the research of Ly et al. [47] concluded that the treatment of *S. japonica* by dilute nitric acid may not only eliminated inorganics but also removed some soluble compounds from the biomass material and chemically changed the structure of the biomass sample. That research focused on catalytic fast pyrolysis in a fluidized-bed reactor and showed an increase in liquid yield and a decrease in char yield by increasing the concentration of nitric acid from 0 to 5 %. Therefore, when utilizing bark as a feedstock for a depolymerization process pretreatment before use can significantly enhance the liquid bio-oil yield.

3.4. Liquid product characterization

The detected liquid components through 2D-GCMS analysis are presented in Table S3, Figure S6 and Fig. 5. The detected liquid components were divided into groups containing aliphatic alcohols/ketones/acids, cycloalkanes, saturated cyclic alcohols/ketones, aromatics, phenolics, furans, and naphthenic/biphenyl components. The blank test at 350 °C-20 bar of H_2 showed high yields of aliphatic alcohols/ketones/acids (19.7 wt%), and phenolic compounds (21.3 wt%), as seen in Fig. 5 (A). Without catalyst, clearly only thermal cracking reactions occurred, with mostly phenolics and aliphatic alcohols and ketones. When the NiMo@YNAC (50:50) catalyst was applied in the reaction system and the reaction temperature was increased from 350 to 400 °C, depolymerization and deoxygenation effects were improved. Both aliphatic and saturated cyclic alcohols/ketones yields were decreased from 5.1 to 0.0 wt% and from 7.3 to 1.8 wt%, respectively. On the other hand, the phenolic and aromatic yields increased from 13.7 to 24.9 wt%, and from 0.9 to 16.8 wt%, respectively. The cycloalkane yield also increased from 21.4 to 27.3 up to 375 °C, but then decreased to 19.4 wt% at 400 °C. The deoxygenation effect was favorable at 400 °C, however, the thermal cracking also strongly occurred at high temperature leading to a decrease in aliphatic and cyclic alcohol/ketone yield. Compared to the NiMo supported on Y and NAC alone, the mixtures (YNAC) of these supports (20 wt% NiMo catalyst loading), gave the higher yields of cycloalkanes and aromatics. The NiMo@YNAC with Y/NAC = 25/75 and Y/NAC = 75/25 gave large amount of cycloalkanes (29.8 wt% and 32.2 wt%, respectively), while Y/NAC = 50/50 gave larger amount of aromatics, as seen in Fig. 5(B). The synergetic effect between these two supports improved the deoxygenation and hydrogenation reactions in the system. The use of 30 wt% loading in the reactor of NiMo@YNAC (75:25), 20 bar H_2, 400 °C and 4 h of reaction time gave the most effective results with 48.1 wt% of cycloalkanes and 2.1 wt% of aromatic yields (Fig. 5(C)). The total yield of deoxygenated products was 50.2 wt % at these conditions. When the H_2 pressure at room temperature was increased to 35 bar, the saturated cyclic alcolhol/ketones yield increased to 12.2 wt%, whereas the yield of cycloalkanes decreased slightly to 36.4 wt%, respectively (Fig. 5(D)). Surprisingly, with increased pressure the deoxygenation effect slightly decreased, whereas the hydrogenation effect was more favored compared to the 20 bar H_2 results. The other types of supports tested, such as CeO_2, TiO_2, and ZrO_2 showed lower catalytic effects on the monomeric and deoxygenated product yields except γ-Al_2O_3 (Fig. 5(E)). Specifically, 30.8 wt% of cycloalkanes and 12.1 wt% of aromatic yields were obtained among monomeric products using NiMo@γ-Al_2O_3. On the other hand, the phenolic contents increased when the other supports were utilized. This indicated that the deoxygenation effect decreased as follows: γ-Al_2O_3>ZrO_2>TiO_2>CeO_2 with the other supports.

Compared to sawdust, bark was clearly more difficult to depolymerize into deoxygenated products, as seen in Fig. 5(F). Through the

RCL process, bark was converted into monomers yielding 10.7 wt% cycloalkanes, 2.2 wt% aromatics, and 34.8 wt% phenolic compounds. The total yield of deoxygenated products obtained was about 12.9 wt%. Since bark has lower amount of volatile matter and higher inorganic contents (Table S1), bark is more difficult to depolymerize. We have therefore pretreated the bark using 5 % HNO_3 to reduce extractive and inorganic contents, which favored the depolymerization process (see Fig. 4). With this pretreatment, the total detected monomeric yield increased to 67.8 wt% which included 19.5 wt% cycloalkanes, 2.2 wt% aromatics, 30.4 wt% phenolics, and 9.1 wt% furanic compounds.

The high molecular weight liquid components (heavy oil fraction), undetectable by 2D-GCMS, were resolved using 2D-NMR-HSQC and GPC analysis (Fig. 6). The molecular weight of the heavy oil fraction from RCL of sawdust and bark at 400 °C ranged from 1588 to 716 g/mol. The molecular weight of the heavy oil fraction (Fig. 6(B)) was generally inversely correlated with the monomer fraction yield of the liquid oil (Fig. 4), where lower monomer yields resulted in a higher molecular weight of the heavy oil fraction. This is reasonable, since conditions with poorer RCL in this case gives both less monomers and that the heavy components are larger. Methods described in the literature were used to identify and label the peaks and regions of the 2D-NMR-HSQC spectra that corresponded to various functional groups [51,52]. The heavy fraction from sawdust with the reaction conditions of 30 wt% loading of NiMo@YNAC (75:25) at 400 °C–4 h – 20 bar H_2 showed mainly aromatic and unsaturated C-H's (phenanthreolines and polycyclic components), as evident in Fig. 6(A). Particularly, two isolated areas with distinctly downfield proton (δ^1H ca. 6.3–7.8 ppm) and carbon (δ^{13}C ca. 110–135 ppm) chemical shifts are characteristic of phenanthrenes and polycyclic aromatics. Those components were a combination of tricin, guaiacyl, syringyl, ferulate, p-coumarate, and p-hydroxylphenyl units [51,53]. This indicated that the repolymerization reactions mainly occurred due to the involvement of lignin-derived fragments and thus, formed higher molecular weight compounds during the charring process.

The reaction pathways for forest residues depolymerization are also proposed in Fig. 7. By catalytic liquefaction, the biomass was first decomposed into a tar phase, then the tar phase was further broken down into monomer compositions (bio-oils) and/or condensed into higher molecular weight components to form char. The experimentally observed heavy oil product fraction, found above by NMR analysis to contain biomass-derived fragments, should represent this partially decomposed biomass or tar. The bio-oil could also condense to generate macro-molecular compounds through coupling reactions to produce char later in the process. On the other hand, bio-oil was hydrogenated to produce cyclic/saturated compounds and then deoxygenated into monocyclic saturated hydrocarbons or directly deoxygenated by dehydration, demethoxylation, decarboxylation, and decarbonylation to generate monoaromatic hydrocarbons. In the final stage, these monoaromatic hydrocarbons were hydrogenated to form monocyclic saturated hydrocarbons. The gas products such as CO_2, CO, C_1-C_4 oxygenates and hydrocarbons were generated by cracking, decarboxylation, and decarbonylation reactions.

3.5. Catalyst deactivation and regeneration

The primary cause of catalyst deactivation was presumably due to bulky organics, coke/char, or ash and tar blocking some of the active sites and pore channels [32,54]. The spent catalyst was named S-NiMo@YNAC (72:25) and the regenerated catalysts are named R1, R2, and R3 corresponding to the number of regeneration cycles. Catalyst regeneration involved rinsing with acetone followed by heat treatment in Ar at 600 °C (details in Section 1.1). According to Table 2 and Fig. S7, the surface area, pore size, and pore volume of the spent catalyst were 77.0 m^2/g, 6.84 nm, and 0.16 cm^3/g respectively. Compared to the fresh catalyst, the spent catalyst had a significantly lower surface area and pore volume, but a larger average pore size. The coke plugs/blocks small pores of catalyst, however, the coke also could form its own larger pores when enough accumulates on the surface of the catalyst. Fig. 8 presents the characterization results of the spent catalyst by XRD, and TGA/TPO analysis. Through XRD, the difference between spent and fresh catalyst (see Fig. 1) was not clearly observed, however small peaks of MoO_2 were observed on the spent catalyst at 25.8°, 53.4°, and 36.8°. The reduced Mo might be partially converted into the MoO_2 phase due to the deoxygenation reactions. By comparing the weight loss of fresh and spent catalysts using thermogravimetric analysis with air, it is possible to determine the amount of carbonaceous material deposited on the spent catalyst. The catalysts were heated at a rate of 10 °C/min from room temperature to 700 °C. The fresh catalyst lost 20 wt% of its weight under TGA, whereas the spent catalyst lost 31.2 wt%. This comparison shows

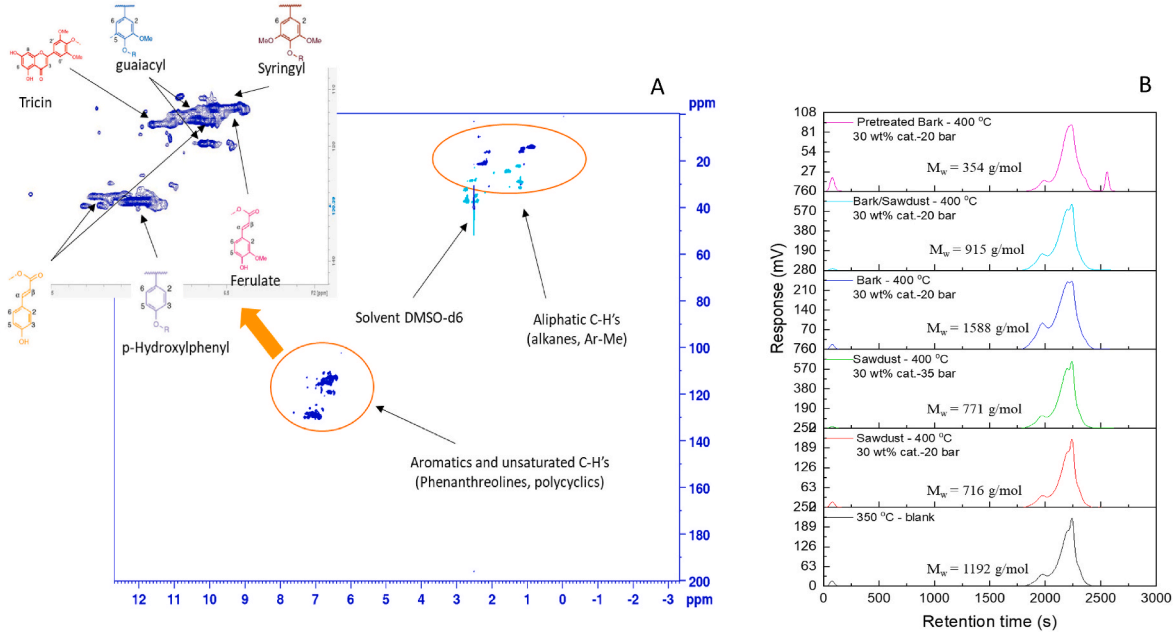

Fig. 6. Characterization of heavy oil fraction: (A) 2D-NMR spectra of heavy fraction from sawdust depolymerization using 30 wt% NiMo@YNAC (75:25) at 400 °C – 4h–20 bar H_2 conditions, (B) Mass average molecular weights of heavy fraction under chosen conditions.

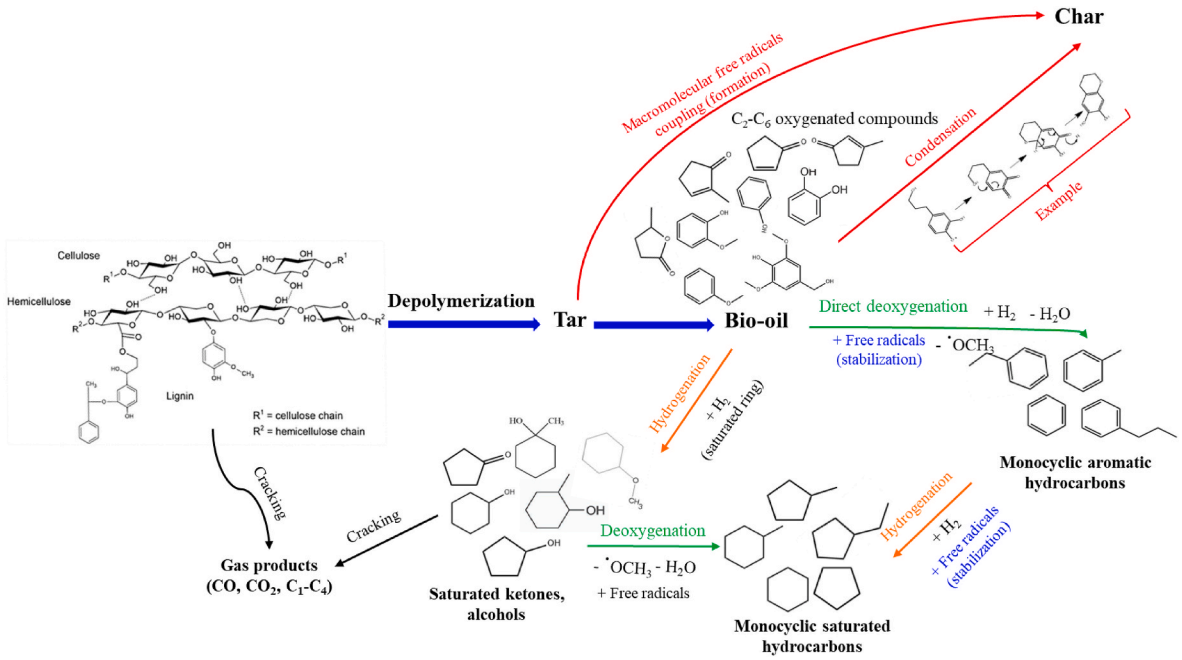

Fig. 7. Reaction pathways of biomass depolymerization during catalytic liquefaction.

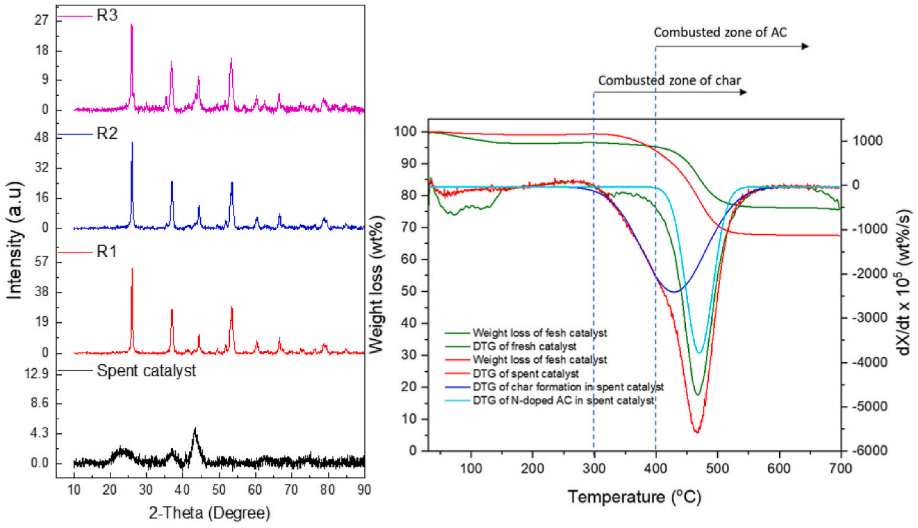

Fig. 8. XRD and TGA/TPO profiles of spent and regenerated catalysts.

that 11.2 wt% of the weight of the spent catalyst was coke/char material. The location and composition of the coke influences the variation in temperature of its combustion. The inside coke is said to burn at a higher temperature than the external coke [21,32]. It has been reported that the external coke is burned at above 300 °C and the internal coke/activated carbon is burned at higher than about 400 °C [21].

The surface area of regenerated catalysts R1, R2, R3 decreased from 214.0 to 66.1 m^2/g, and pore volume decreased from 0.23 to 0.03 cm^3/g, respectively (Table 2). Meanwhile, the pore size of the regenerated catalysts was almost constant at about 6.9 nm. The first regeneration cycle (R1) recovered the surface area of the fresh catalyst. Probably, a good part of the deposited carbon was removed with this first regeneration, but with following cycles the surface areas dropped indicating that more recalcitrant carbon eventually accumulates. The XRD patterns in Fig. 8 of R1, R2, R3 showed high crystallinity of the Ni and Mo oxides after the regeneration steps. The peaks at 44.4° and 51.7° represent Ni while the peaks at 25.9, 36.9, and 53.6° represent MoO_2, respectively. Mo_3Ni_2N was observed through the peaks at 40.7, 43, and 45.3°, respectively. Fig. 9 shows that the catalytic effect for the three reaction cycles using sawdust, steadily decreased due to the increasing solid yield and decreasing liquid oil yields. The solid products during the three cycles increased from 12.2 to 22.0 wt%, whereas the liquid oil decreased from 81.1 to 71.1 wt%, whereas the gas yield was almost stable at around 7.0 wt%. The water content decreased from 3.0 to 2.5 wt%. The deoxygenation effect was decreased due to the high crystallinity of the active phase and increasing accumulation of recalcitrant carbon formation on the surface of the catalyst which resulted in a decrease of cycloalkanes and aromatics yields to 10.8 wt%, whereas the phenolic yield was increased to about 33.0 wt%. The average molecular weight of the heavy fraction through the three cycles increased from 981 to 1355 g/mol, as its yield increased from 9.0 to 16.3 wt%.

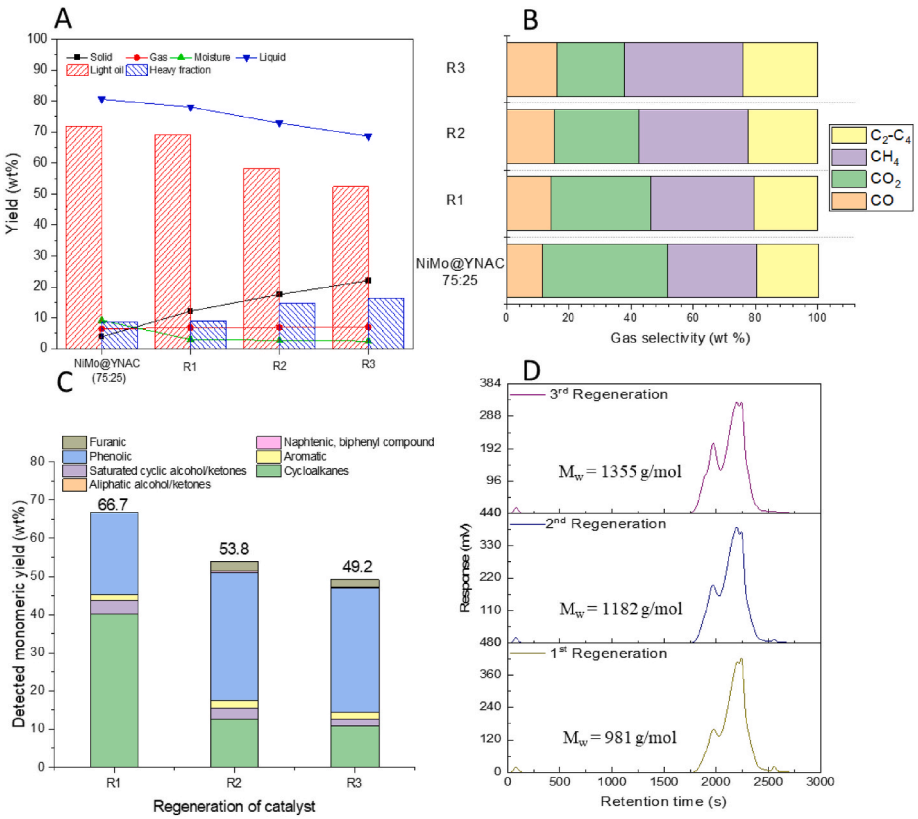

Fig. 9. Product analysis using regenerated catalysts after 3 cycles using 30 wt% of catalyst at 400 °C, 20 bar of H_2 (room temperature), 4 h, using sawdust: (A) Product distribution, (B) Gas product compositions, (C) GC Detected monomeric yield, (D) Molecular weight distribution of heavy fraction.

4. Conclusions

A one-pot reductive depolymerization of sawdust and bark into bio-oils was investigated using NiMo catalysts on various supports under different reaction conditions. The use of a 30 wt% loading of NiMo@YNAC(75:25) catalyst at 400 °C and 20 bar H_2 (at room temperature) for 4 h was most effective for the depolymerization of the biomass samples with the lowest yield of solid byproducts, compared to the other catalysts and conditions investigated. The lowest solid yields from sawdust, bark, and blended sawdust/bark (8/2 wt ratio) feedstocks were 3.9, 18.2, and 8.4 wt%, respectively. The total yield of deoxygenated products achieved was 50.2 wt%, of which 48.1 wt% were cycloalkane compounds, amounting to a total monomer yield of 71.9 wt % with the most effective conditions using the sawdust feedstock. The use of different supports for the NiMo catalyst (γ-Al_2O_3, TiO_2, CeO_2, and ZrO_2) resulted in lower bio-oils yields compared to the NiMo@YNAC (75:25) catalyst, with higher solid yields and similar gas yields. In addition, compared to the NiMo on the two parent supports (Y, NAC), the NiMo@YNAC (75:25) catalyst was more efficient for both depolymerization and deoxygenation into bio-oils, especially cycloalkane products, which potentially could be used in sustainable aviation fuels (SAF). The good performance of the hybrid support (YNAC) can be linked to its combination of both acidic and basic sites.

Furthermore, the results also suggest that with the use of bark as feedstock, a pretreatment step can be used to reduce the ash and extractives content which results in a decreased solid yield (from 18 % to 6 %), and improved yields of liquid products (from 78 % to 91 %).

CRediT authorship contribution statement

Quoc Khanh Tran: Writing – original draft, Supervision, Methodology, Investigation, Formal analysis, Conceptualization. **Muhammad Abdus Salam:** Methodology, Formal analysis, Data curation. **Phuoc Hoang Ho:** Methodology, Investigation, Formal analysis, Data curation. **Huy Xuan Le:** Methodology, Investigation, Formal analysis. **Christian Kugge:** Writing – review & editing, Methodology, Conceptualization. **Derek Creaser:** Writing – review & editing, Supervision, Methodology, Conceptualization. **Louise Olsson:** Writing – review & editing, Supervision, Conceptualization.

Declaration of competing interest

The authors declare that they have no known competing financial interests or personal relationships that could have appeared to influence the work reported in this paper.

Acknowledgements

This work is a collaboration between Chemical Engineering at Chalmers and SCA. We would like to acknowledge Swedish Energy Agency (P52405-1), Formas (2021-01676) and Bo Rydin foundation for the funding.

Appendix A. Supplementary data

Supplementary data to this article can be found online at https://doi.org/10.1016/j.renene.2025.122835.

References

[1] D. Lee, H. Nam, M. Won Seo, S. Hoon Lee, D. Tokmurzin, S. Wang, Y.-K. Park, Recent progress in the catalytic thermochemical conversion process of biomass for biofuels, Chem. Eng. J. 447 (2022) 137501, https://doi.org/10.1016/j.cej.2022.137501.

[2] J.-Y. Kim, H.W. Lee, S.M. Lee, J. Jae, Y.-K. Park, Overview of the recent advances in lignocellulose liquefaction for producing biofuels, bio-based materials and

chemicals, Bioresour. Technol. 279 (2019) 373–384, https://doi.org/10.1016/j.biortech.2019.01.055.
[3] G.T. Jaya, R. Insyani, J. Park, A.F. Barus, M.G. Sibi, V. Ranaware, D. Verma, J. Kim, One-pot conversion of lignocellulosic biomass to ketones and aromatics over a multifunctional Cu–Ru/ZSM-5 catalyst, Appl. Catal. B Environ. 312 (2022) 121368, https://doi.org/10.1016/j.apcatb.2022.121368.
[4] L.R. Lynd, G.T. Beckham, A.M. Guss, L.N. Jayakody, E.M. Karp, C. Maranas, R. L. McCormick, D. Amador-Noguez, Y.J. Bomble, B.H. Davison, C. Foster, M. E. Himmel, E.K. Holwerda, M.S. Laser, C.Y. Ng, D.G. Olson, Y. Román-Leshkov, C. T. Trinh, G.A. Tuskan, V. Upadhayay, D.R. Vardon, L. Wang, C.E. Wyman, Toward low-cost biological and hybrid biological/catalytic conversion of cellulosic biomass to fuels, Energy Environ. Sci. 15 (2022) 938–990, https://doi.org/10.1039/D1EE02540F.
[5] J. Park, U. Mushtaq, J.R. Sugiarto, D. Verma, J. Kim, Total chemocatalytic cascade conversion of lignocellulosic biomass into biochemicals, Appl. Catal. B Environ. 310 (2022) 121280, https://doi.org/10.1016/j.apcatb.2022.121280.
[6] Q. Zhao, M. Mäkinen, A. Haapala, J. Jänis, Thermochemical conversion of birch bark by temperature-programmed slow pyrolysis with fractional condensation, J. Anal. Appl. Pyrolysis 150 (2020) 104843, https://doi.org/10.1016/j.jaap.2020.104843.
[7] M.W. Seo, S.H. Lee, H. Nam, D. Lee, D. Tokmurzin, S. Wang, Y.-K. Park, Recent advances of thermochemical conversion processes for biorefinery, Bioresour. Technol. 343 (2022) 126109, https://doi.org/10.1016/j.biortech.2021.126109.
[8] W. Chou, D. Liu, W. Li, X. Chou, H. Liu, C. Wu, P. Wu, Z. Men, Z. Li, Full utilization of lignocellulose through one-pot in-situ hydro-liquefaction with versatile Pt/CeCrO2−x catalyst, Appl. Catal. B Environ. 316 (2022) 121625, https://doi.org/10.1016/j.apcatb.2022.121625.
[9] M.M. Abu-Omar, K. Barta, G.T. Beckham, J.S. Luterbacher, J. Ralph, R. Rinaldi, Y. Román-Leshkov, J.S.M. Samec, B.F. Sels, F. Wang, Guidelines for performing lignin-first biorefining, Energy Environ. Sci. 14 (2021) 262–292, https://doi.org/10.1039/D0EE02870C.
[10] D.G. Brandner, J.S. Kruger, N.E. Thornburg, G.G. Facas, J.K. Kenny, R.J. Dreiling, A.R.C. Morais, T. Renders, N.S. Cleveland, R.M. Happs, R. Katahira, T.B. Vinzant, D.G. Wilcox, Y. Román-Leshkov, G.T. Beckham, Flow-through solvolysis enables production of native-like lignin from biomass, Green Chem. 23 (2021) 5437–5441, https://doi.org/10.1039/D1GC01591E.
[11] E.O. Ebikade, N. Samulewicz, S. Xuan, J.D. Sheehan, C. Wu, D.G. Vlachos, Reductive catalytic fractionation of agricultural residue and energy crop lignin and application of lignin oil in antimicrobials, Green Chem. 22 (2020) 7435–7447, https://doi.org/10.1039/D0GC02781B.
[12] E.M. Anderson, R. Katahira, M. Reed, M.G. Resch, E.M. Karp, G.T. Beckham, Y. Román-Leshkov, Reductive catalytic fractionation of corn stover lignin, ACS Sustain. Chem. Eng. 4 (2016) 6940–6950, https://doi.org/10.1021/acssuschemeng.6b01858.
[13] E. Cooreman, T. Vangeel, K. Van Aelst, J. Van Aelst, J. Lauwaert, J.W. Thybaut, S. Van den Bosch, B.F. Sels, Perspective on overcoming scale-up hurdles for the reductive catalytic fractionation of lignocellulose biomass, Ind. Eng. Chem. Res. 59 (2020) 17035–17045, https://doi.org/10.1021/acs.iecr.0c02294.
[14] T. Vangeel, T. Renders, K. Van Aelst, E. Cooreman, S. Van den Bosch, G. Van den Bossche, S.F. Koelewijn, C.M. Courtin, B.F. Sels, Reductive catalytic fractionation of black locust bark, Green Chem. 21 (2019) 5841–5851, https://doi.org/10.1039/C9GC02139F.
[15] S. Muangmeesri, N. Li, D. Georgouvelas, P. Ouagne, V. Placet, A.P. Mathew, J.S. M. Samec, Holistic valorization of hemp through reductive catalytic fractionation, ACS Sustain. Chem. Eng. 9 (2021) 17207–17213, https://doi.org/10.1021/acssuschemeng.1c06607.
[16] X. Li, T. Guo, Q. Xia, X. Liu, Y. Wang, One-pot catalytic transformation of lignocellulosic biomass into alkylcyclohexanes and polyols, ACS Sustain. Chem. Eng. 6 (2018) 4390–4399, https://doi.org/10.1021/acssuschemeng.8b00012.
[17] I. Klein, B. Saha, M.M. Abu-Omar, Lignin depolymerization over Ni/C catalyst in methanol, a continuation: effect of substrate and catalyst loading, Catal. Sci. Technol. 5 (2015) 3242–3245, https://doi.org/10.1039/C5CY00490J.
[18] Q. Song, F. Wang, J. Cai, Y. Wang, J. Zhang, W. Yu, J. Xu, Lignin depolymerization (LDP) in alcohol over nickel-based catalysts via a fragmentation–hydrogenolysis process, Energy Environ. Sci. 6 (2013) 994–1007, https://doi.org/10.1039/C2EE23741E.
[19] B. Kusserow, S. Schimpf, P. Claus, Hydrogenation of glucose to sorbitol over nickel and ruthenium catalysts, Adv. Synth. Catal. 345 (2003) 289–299, https://doi.org/10.1002/adsc.200390024.
[20] W. Jin, L. Pastor-Pérez, J.J. Villora-Picó, M.M. Pastor-Blas, J.A. Odriozola, A. Sepúlveda-Escribano, T.R. Reina, In-situ HDO of guaiacol over nitrogen-doped activated carbon supported nickel nanoparticles, Appl. Catal. Gen. 620 (2021) 118033, https://doi.org/10.1016/j.apcata.2021.118033.
[21] Q.K. Tran, H.V. Ly, B. Kwon, S.-S. Kim, J. Kim, Catalytic hydrodeoxygenation of guaiacol as a model compound of woody bio-oil over Fe/AC and Ni/γ-Al2O3 catalysts, Renew. Energy 173 (2021) 886–895, https://doi.org/10.1016/j.renene.2021.03.138.
[22] W. Jin, J.L. Santos, L. Pastor-Perez, S. Gu, M.A. Centeno, T.R. Reina, Noble metal supported on activated carbon for “hydrogen free” HDO reactions: exploring economically advantageous routes for biomass valorisation, ChemCatChem 11 (2019) 4434–4441, https://doi.org/10.1002/cctc.201900841.
[23] C. Guizani, O. Sorsa, V. Siipola, T. Ohra-Aho, R. Paalijärvi, A. Pasanen, M. Mäkelä, A. Kalliola, M. Vilkman, K. Torvinen, The effects of lignin structure on the multiscale properties and electrochemical performance of activated carbons, Biomass Conversion and Biorefinery (2023), https://doi.org/10.1007/s13399-023-04373-9.
[24] H.V. Ly, J.W. Park, S.-S. Kim, H.T. Hwang, J. Kim, H.C. Woo, Catalytic pyrolysis of bamboo in a bubbling fluidized-bed reactor with two different catalysts: HZSM-5 and red mud for upgrading bio-oil, Renew. Energy 149 (2020) 1434–1445, https://doi.org/10.1016/j.renene.2019.10.141.
[25] Y. Li, D. Yellezuome, R. Liu, J. Cai, Y. Gao, Investigation of product selectivity and kinetics of poplar sawdust catalytic pyrolysis over bi-metallic Iron-Nickel/ZSM-5 catalyst, Bioresour. Technol. 349 (2022) 126838, https://doi.org/10.1016/j.biortech.2022.126838.
[26] C.A. Mullen, A.A. Boateng, Production of aromatic hydrocarbons via catalytic pyrolysis of biomass over Fe-modified HZSM-5 zeolites, ACS Sustain. Chem. Eng. 3 (2015) 1623–1631, https://doi.org/10.1021/acssuschemeng.5b00335.
[27] M.A. Salam, P. Arora, H. Ojagh, Y.W. Cheah, L. Olsson, D. Creaser, NiMoS on alumina-USY zeolites for hydrotreating lignin dimers: effect of support acidity and cleavage of C–C bonds, Sustain. Energy Fuels 4 (2020) 149–163, https://doi.org/10.1039/C9SE00507B.
[28] M. Abdus Salam, Y. Wayne Cheah, P. Hoang Ho, D. Bernin, A. Achour, E. Nejadmoghadam, O. Öhrman, P. Arora, L. Olsson, D. Creaser, Elucidating the role of NiMoS-USY during the hydrotreatment of Kraft lignin, Chem. Eng. J. 442 (2022) 136216, https://doi.org/10.1016/j.cej.2022.136216.
[29] A. Demirbaş, Calculation of higher heating values of biomass fuels, Fuel 76 (1997) 431–434, https://doi.org/10.1016/S0016-2361(97)85520-2.
[30] K.N. Papageridis, N.D. Charisiou, S. Douvartzides, V. Sebastian, S.J. Hinder, M. A. Baker, A.A. AlKhoori, S.I. AlKhoori, K. Polychronopoulou, M.A. Goula, Continuous selective deoxygenation of palm oil for renewable diesel production over Ni catalysts supported on Al2O3 and La2O3–Al2O3, RSC Adv. 11 (2021) 8569–8584, https://doi.org/10.1039/D0RA08541C.
[31] K.G. Kalogiannis, S.D. Stefanidis, S.A. Karakoulia, K.S. Triantafyllidis, H. Yiannoulakis, C. Michailof, A.A. Lappas, First pilot scale study of basic vs acidic catalysts in biomass pyrolysis: deoxygenation mechanisms and catalyst deactivation, Appl. Catal. B Environ. 238 (2018) 346–357, https://doi.org/10.1016/j.apcatb.2018.07.016.
[32] Q.K. Tran, S. Han, H.V. Ly, S.-S. Kim, J. Kim, Hydrodeoxygenation of a bio-oil model compound derived from woody biomass using spray-pyrolysis-derived spherical γ-Al2O3-SiO2 catalysts, J. Ind. Eng. Chem. 92 (2020) 243–251, https://doi.org/10.1016/j.jiec.2020.09.012.
[33] E.A. Couto, F. Pinto, F. Varela, A. Reis, P. Costa, M.L. Calijuri, Hydrothermal liquefaction of biomass produced from domestic sewage treatment in high-rate ponds, Renew. Energy 118 (2018) 644–653, https://doi.org/10.1016/j.renene.2017.11.041.
[34] A. Achour, D. Bernin, D. Creaser, L. Olsson, Evaluation of kraft and hydrolysis lignin hydroconversion over unsupported NiMoS catalyst, Chem. Eng. J. 453 (2023) 139829, https://doi.org/10.1016/j.cej.2022.139829.
[35] P. Sirous-Rezaei, D. Creaser, L. Olsson, Reductive liquefaction of lignin to monocyclic hydrocarbons: ReS2/Al2O3 as efficient char inhibitor and hydrodeoxygenation catalyst, Appl. Catal. B Environ. 297 (2021) 120449, https://doi.org/10.1016/j.apcatb.2021.120449.
[36] R. Insyani, J.-W. Choi, C.-J. Yoo, D.J. Suh, H. Lee, K. Kim, C.S. Kim, K.H. Kim, J.-M. Ha, Improved hydrodeoxygenation of lignin-derived oxygenates and biomass pyrolysis oil into hydrocarbon fuels using titania-supported nickel phosphide catalysts, Energy Convers. Manag. 266 (2022) 115822, https://doi.org/10.1016/j.enconman.2022.115822.
[37] C. Yuan, S. Wang, B. Cao, Y. Hu, A.E.-F. Abomohra, Q. Wang, L. Qian, L. Liu, X. Liu, Z. He, C. Sun, Y. Feng, B. Zhang, Optimization of hydrothermal co-liquefaction of seaweeds with lignocellulosic biomass: merging 2nd and 3rd generation feedstocks for enhanced bio-oil production, Energy 173 (2019) 413–422, https://doi.org/10.1016/j.energy.2019.02.091.
[38] D. Zhou, L. Zhang, S. Zhang, H. Fu, J. Chen, Hydrothermal liquefaction of macroalgae enteromorpha prolifera to bio-oil, Energy & Fuels 24 (2010) 4054–4061, https://doi.org/10.1021/ef100151h.
[39] W.-T. Chen, Y. Zhang, J. Zhang, G. Yu, L.C. Schideman, P. Zhang, M. Minarick, Hydrothermal liquefaction of mixed-culture algal biomass from wastewater treatment system into bio-crude oil, Bioresour. Technol. 152 (2014) 130–139, https://doi.org/10.1016/j.biortech.2013.10.111.
[40] M. Grilc, B. Likozar, J. Levec, Simultaneous liquefaction and hydrodeoxygenation of lignocellulosic biomass over NiMo/Al2O3, Pd/Al2O3, and zeolite Y catalysts in hydrogen donor solvents, ChemCatChem 8 (2016) 180–191, https://doi.org/10.1002/cctc.201500840.
[41] N.H. Zainan, S.C. Srivatsa, F. Li, S. Bhattacharya, Quality of bio-oil from catalytic pyrolysis of microalgae Chlorella vulgaris, Fuel 223 (2018) 12–19, https://doi.org/10.1016/j.fuel.2018.02.166.
[42] Z. Geng, C. Zhang, D. Wang, X. Zhou, M. Cai, Pore size effects of nanoporous carbons with ultra-high surface area on high-pressure hydrogen storage, J. Energy Chem. 24 (2015) 1–8, https://doi.org/10.1016/S2095-4956(15)60277-7.
[43] J. Li, J. Zhang, S. Wang, G. Xu, H. Wang, D.G. Vlachos, Chemoselective hydrodeoxygenation of carboxylic acids to hydrocarbons over nitrogen-doped carbon–alumina hybrid supported iron catalysts, ACS Catal. 9 (2019) 1564–1577, https://doi.org/10.1021/acscatal.8b04967.
[44] D. Liu, L. Song, P. Wu, Y. Liu, Q. Li, Z. Yan, Direct hydro-liquefaction of sawdust in petroleum ether and comprehensive bio-oil products analysis, Bioresour. Technol. 155 (2014) 152–160, https://doi.org/10.1016/j.biortech.2013.12.076.
[45] T.W. van Deelen, C. Hernández Mejía, K.P. de Jong, Control of metal-support interactions in heterogeneous catalysts to enhance activity and selectivity, Nat. Catal. 2 (2019) 955–970, https://doi.org/10.1038/s41929-019-0364-x.
[46] H. Zhang, S. Fu, X. Du, Y. Deng, Advances in versatile nanoscale catalyst for the reductive catalytic fractionation of lignin, ChemSusChem 14 (2021) 2268–2294, https://doi.org/10.1002/cssc.202100067.

[47] H.V. Ly, J.H. Choi, H.C. Woo, S.-S. Kim, J. Kim, Upgrading bio-oil by catalytic fast pyrolysis of acid-washed Saccharina japonica alga in a fluidized-bed reactor, Renew. Energy 133 (2019) 11–22, https://doi.org/10.1016/j.renene.2018.09.103.
[48] J.-W. Park, J. Heo, H.V. Ly, J. Kim, H. Lim, S.-S. Kim, Fast pyrolysis of acid-washed oil palm empty fruit bunch for bio-oil production in a bubbling fluidized-bed reactor, Energy 179 (2019) 517–527, https://doi.org/10.1016/j.energy.2019.04.211.
[49] I. Miranda, J. Gominho, I. Mirra, H. Pereira, Fractioning and chemical characterization of barks of Betula pendula and Eucalyptus globulus, Ind. Crop. Prod. 41 (2013) 299–305, https://doi.org/10.1016/j.indcrop.2012.04.024.
[50] S. Rasi, P. Kilpeläinen, K. Rasa, R. Korpinen, J.-E. Raitanen, M. Vainio, V. Kitunen, H. Pulkkinen, T. Jyske, Cascade processing of softwood bark with hot water extraction, pyrolysis and anaerobic digestion, Bioresour. Technol. 292 (2019) 121893, https://doi.org/10.1016/j.biortech.2019.121893.
[51] H. Ben, A.J. Ragauskas, Comparison for the compositions of fast and slow pyrolysis oils by NMR characterization, Bioresour. Technol. 147 (2013) 577–584, https://doi.org/10.1016/j.biortech.2013.07.151.
[52] N. Sudasinghe, J.R. Cort, R. Hallen, M. Olarte, A. Schmidt, T. Schaub, Hydrothermal liquefaction oil and hydrotreated product from pine feedstock characterized by heteronuclear two-dimensional NMR spectroscopy and FT-ICR mass spectrometry, Fuel 137 (2014) 60–69, https://doi.org/10.1016/j.fuel.2014.07.069.
[53] W. Mu, H. Ben, G. Newalkar, A. Ragauskas, D. Qiu, Y. Deng, Structure analysis of pine bark-, residue-, and stem-derived light oil and its hydrodeoxygenation products, Ind. Eng. Chem. Res. 53 (2014) 11269–11275, https://doi.org/10.1021/ie500541p.
[54] Y. Huang, Y. Duan, S. Qiu, M. Wang, C. Ju, H. Cao, Y. Fang, T. Tan, Lignin-first biorefinery: a reusable catalyst for lignin depolymerization and application of lignin oil to jet fuel aromatics and polyurethane feedstock, Sustain. Energy Fuels 2 (2018) 637–647, https://doi.org/10.1039/C7SE00535K.